Evaluation of resorbable polydioxanone and polyglycolic acid meshes in a rat model of ventral hernia repair

Timur Fatkhudinov [ID],[1,2] Larisa Tsedik,[3] Irina Arutyunyan,[1,4] Anastasia Lokhonina,[1,4]
Andrey Makarov [ID],[1,5] Aleksey Korshunov,[1] Andrey Elchaninov,[1,5] Evgeniya Kananykhina,[1,4]
Olesya Vasyukova,[1,4] Natalia Usman,[1] Elena Uvarova,[1] Vladimir Chuprynin,[1] Irina Eremina,[2]
Dmitry Degtyarev,[1] Gennady Sukhikh[1]

[1]National Medical Research Center for Obstetrics, Gynecology and Perinatology named after Academician V.I. Kulakov of
Ministry of Healthcare of Russian Federation, Moscow, Russia
[2]Peoples' Friendship University of Russia, Moscow, Russia
[3]State Scientific Institution «Powder Metallurgy Institute», Minsk, Republic of Belarus
[4]Research Institute of Human Morphology, Moscow, Russia
[5]Pirogov Russian National Research Medical University, Ministry of Healthcare of Russian Federation, Moscow, Russia

Abstract: The objective of this study was to evaluate physical, mechanical, and biological properties of the polydioxanone (PDO) monofilament meshes and polyglycolide (PGA) polyfilament meshes in comparison with Permacol® implants. In rat experimental model, a 1.5×2.0 cm defect in abdominal wall was reconstructed by using the Permacol surgical implant or knitted meshes produced from either PDO monofilament, or PGA multifilament. The implant sites were assessed for the tensile strength and the extents of material resorption, host inflammatory response and host tissue replacement on days 3, 10, 30, or 60 after the surgery. The PDO and PGA meshes were rapidly pervaded by the host connective tissue with elements of skeletal muscle histogenesis. The degree of adhesions was significantly higher in the Permacol group. All of the prostheses underwent resorption, which correlated with gradual decreases in the overall tensile strength of the site and the *Col1a1* gene expression level.

Elevated expression of *Fgf2* gene maintained longer in the PDO group, and the *Mmp9* gene expression level in this group was higher than in the other groups. Gene expression levels of inflammatory cytokines were higher in the Permacol group. The foreign body giant cell numbers were lower in the PDO and Permacol groups than in the PGA group. Minimal macrophage infiltration with predominance of M2 cells was observed in the PDO group. Overall, the PDO prosthesis turned out to be significantly better than the PGA or Permacol prostheses by a number of indicators of biocompatibility and efficacy. © 2018 The Authors Journal of Biomedical Materials Research Part B: Applied Biomaterials Published by Wiley Periodicals, Inc. J Biomed Mater Res Part B: Appl Biomater 107B: 652–663, 2019.

Key Words: animal model, biocompatibility/soft tissue, cell–material interactions, cytokines, resorbable mesh

INTRODUCTION

Permanent surgical prostheses based on various non-resorbable polymer materials are widely used in abdominal wall hernia repair and pelvic floor reinforcement.[1–3] Utilization of synthetic (predominantly polypropylene) surgical meshes significantly reduces the risk of recurrence, as compared with grafting of patient's own tissue in surgical treatment of hernias and pelvic organ prolapses.[3,4] However, their utilization may confer certain postoperative mesh-associated complications related to the inflammatory reaction of tissues to foreign body and manifested as long-term (sometimes life-long) seromas, as well as fibrosis, chronic pains, deformation of the prosthesis, and formation of fistulas and adhesions. Resolution of these complications frequently requires an additional surgical intervention.[5–8]

The resorbable decellularized tissue-based prostheses, derived from skin dermis, intestinal submucosa, and so forth of animals and humans, were proposed as a means to avoid the long-term postoperative complications. Resorption of the prosthesis and its replacement with the host tissues were believed to provide a solution (an implication of the "no prosthesis—no complications" principle). However, the idea did not work out well. By probabilities of hernia recurrence and other postoperative complications, the resorbable

decellularized tissue-based prostheses turned out to be comparable or inferior to their synthetic counterparts.[9–11] The foreign body inflammatory reaction develops independently of the nature of implanted material, either animal tissue-derived, or synthetic.[12] An additional drawback is due to the fact that obtaining of tissue-derived prostheses with appropriate biomechanical properties (i.e., strong enough to withstand the anatomical load) requires artificial introduction of additional cross-links into collagen molecules, which leads to considerable compaction of the material and decreases its porosity, impedes tissue ingrowth, and compromises the engraftment.[9] Besides, the use of biological prostheses of this type is limited by their high costs.

Although the search for the best combinations of materials and designs for hernia repair is still under way,[13] it can be said that the problem will be solved by developing resorbable prostheses that, being as strong and porous as non-resorbable synthetic prostheses, would also be biocompatible.

To date, a few resorbable synthetic prostheses are used in clinical surgery. Of these, the polyglactin Vicryl® meshes (Ethicon) lose their mechanical strength in 2 weeks after the surgery, and, therefore, are suitable for only a temporary support of wound margins or an organ. The polyglycolide (PGA) Dexon® meshes (American Cyanamid) have similar properties. The Tigr Matrix® meshes (Novus Scientific) and Gore Bio-A® Hernia Plug™ non-woven microporous material (Gore) composed of trimethylenecarbonate and PGA copolymer have longer resorption period of up to 9 months. These are suitable for mammoplasty, inguinal hernia and intestinal fistula surgical treatments.[14,15] The Phasix™ ST Mesh (CR Bard, Inc.) is composed of poly-4-hydroxybutyrate, it is resorbed in 52 weeks, and its clinical usage is still limited.[16]

The study was preceded by empirical selection among experimental mesh samples, which differed by the material (polydioxanone [PDO], PGA, polylactide and poly(lactide-co-glycolide)), filament thickness and knitting mode. Sample PDO and PGA meshes produced by warp knitting have been selected because of their high tensile strength, availability, and easy handling meshes produced by warp knitting (the selection procedure is not presented in the article). It is interesting to compare the PDO monofilament and PGA polyfilament designs since they differ by the rates of resorption[17] and will therefore most probably show differential dynamics of the tensile strength at the site of implantation The article evaluates physical, mechanical and biological properties of these meshes in comparison with Permacol®— a widely accepted animal tissue-derived resorbable material for hernioplastics.

METHODS
Materials
The reagents and consumables were obtained from Sigma-Aldrich (Dorset, UK), Abcam (Cambridge, UK), or BioVitrum (St. Petersburg, Russia), unless stated otherwise.

Mesh fabrication
The 1.5 × 2.0 cm meshes were knitted from PDO monofilament (MEPFIL-D, Intraros) or PGA multifilament (MEPFIL, Intraros), both USP 3–0.

Mesh characterization
Assessment of porosity and mechanical properties. Porosity of the meshes was determined by nitrogen adsorption using a SA 3100 surface area and pore size analyzer (Beckman Coulter, CA). The ultimate tensile strength was determined by using a H150KU Tensile Test Machine (Tinius Olsen, UK) at 5 mm/min. The microhardness of the filaments was quantified by atomic force microscopy (ICON) before and after the hydrolytic destruction in phosphate buffer (pH = 7.32) for 30 days.

In vitro cytotoxicity assay. Cytotoxicity of the materials was measured by methylthiazolyldiphenyl-tetrazolium bromide (MTT) test. Human multipotent stromal cells (MSCs) were plated in 96-well plates at 5×10^3 cells per well. Single 5 mm lengths of PDO or PGA yarns were placed in the wells for 1, 2, or 5 days, in parallel with the no-yarn controls. After the incubation, the yarns were removed, and the growth medium was supplemented with MTT (Sigma) to 1 mg/mL final concentration, and the cells were further incubated for 3 h at standard cultural conditions. The medium was subsequently replaced with 100 μL of dimethylsulfoxide (Sigma) as a solvent, and the formazan crystals were allowed to dissolve for 15 min. OD at $\lambda = 570$ nm was measured by Multiskan GO spectrophotometer (Thermo Scientific). Each of the reported values is based on 6-fold measurements in three sequential identical experiments.

Experimental model of the anterior abdominal wall defect
The study was approved by Ethical Review Board at the Institute of Human Morphology (Protocol No. 4, August 8, 2016). The animals were obtained from Institute of Bioorganic Chemistry branch animal facilities (Pushchino, Russia). All experimental work involving animals was carried out according to the standards of laboratory practice (National Guidelines No. 267 by Ministry of Healthcare of the Russian Federation, June 1, 2003), and all possible efforts were made to minimize suffering. A total of 72 mature outbred male Sprague-Dawley rats weighing 250–320 g were used in the study. The rats were randomly subdivided into three groups corresponding to transplantation of either PDO implant, PGA implant, or Permacol (5001–100, Covidien).

The rats were anesthetized with zoletil (20 mg/kg) (Virbac, France) and rometar (5 mg/kg) (Bioveta, Czech Republic). Access to surgical field was provided by applying a 4 cm longitudinal skin incision to the middle of abdomen. A full-thickness rectangular graft of anterior abdominal wall, 1.5 cm wide and 2 cm long, was excised symmetrically relative to the midline demarcated by *linea alba*. The gaping of abdominal cavity was immediately filled with a mesh prosthesis of a matching size with margins of the defect lapping over margins of the prosthesis, and the construction was

secured with continuous suture (Vicril 2–0, Ethicon) around the perimeter. The skin incision was sutured, and the seam was treated with antiseptic, followed by an intramuscular injection of Baralgin M (10 mg/kg) as postoperative analgesia.

The animals were withdrawn from the experiment on day 3, 10, 30, or 60 after the surgery by overdose of anesthetic. Dissected tissues were placed in either 10% buffered formalin for paraffin sectioning, or liquid nitrogen for cryo-sectioning, or 50% ethanol for biomechanical tests.

Postoperative wound healing was scrupulously monitored, and animals with compromised seams, deformed abdominal wall, or eventration of either prosthesis or internal organ(s) were excluded from the experiment. Upon dissection, all animals were subjected to thorough macroscopic examination, and all cases of hematomas, seromas, abscesses, or adhesions in the transplantation area were documented. In particular, the adhesion formation rates were evaluated in points.[18]

Tensiometry

Tensile strength tests were performed using an electromechanical testing machine equipped with SCG-1kNA holding apparatus (Shimadzu, Japan) with 10 mm distance between the grips. The loading rate was set to 5 mm/min, and the breaking point parameters were recorded.

Histological examination

Formalin-fixed specimens were dehydrated, embedded in paraffin, and cut using a manual microtome. The sections, 5–7 μm thick, were stained with H&E. Morphometric study was conducted using Leica DM 4000 B microscope with LAS AF v.3.1.0 build 8587 software (Leica Microsystems) at ×400 magnification images. The measured variables included:

1. Filament diameter (for mesh implants) or thickness (for Permacol), based on at least 100 measurements per group per time-lapse after surgery;
2. Number of foreign-body giant cells in the transplantation area, at the borderline between the mesh and surrounding tissues, based on at least 100 fields of view per group per time-lapse after surgery;
3. Number of nuclei per one foreign-body giant cell based on at least 50 cells per group per time-lapse after surgery.

Immunochemistry

A set of markers selected for immunochemistry included macrophage-specific CD68 (ab125212, Abcam), M2 activated macrophage-specific CD206 (sc-34577, Santa Cruz Biotechnology), collagen type I (RAQ C11, Imtek, Russia), smooth muscle actin (αSMA) (ab5694, Abcam), skeletal muscle-specific troponin I (sc-15368, Santa Cruz Biotechnology). Cryosections were stained with antibodies according to recommendations of the manufacturers. Morphometric study was conducted using Leica DM 4000 B microscope

with LAS AF v.3.1.0 build 8587 software (Leica Microsystems) at ×400 magnification images. Relative counts of CD68+ and CD206+ cells within the transplantation area were calculated for at least 100 fields of view per group per time-lapse after surgery.

Polymerase chain reaction (PCR) analysis of mRNA expression

Total RNA was isolated from tissue samples using RNeasy Plus Mini Kit (QIAGEN, Germany) and immediately transferred to random-primed cDNA synthesis reaction using MMLV RT Kit (Evrogen CJSC, Russia) at 39°C for 1 h.

Polymerase chain reactions were set using commercial qPCRmix-HS SYBR kits (Evrogen CJSC) with 0.2–0.4 μM oligonucleotide primers (SYNTOL, Russia). The primer information is summarized in Table I. Real-time PCR in DT-96 real-time PCR cycler (DNA-Technology JSC, Russia) was carried out at 95°C for 5 min followed by (95°C 15 s, 62° for 10 s +reading, 72° for 20 s)×45, with characteristic values (Cp) generated automatically by nonlinear regression algorithm. Relative mRNA representation values were derived from the raw data by using *actb*, *b2m*, and *gapdh* (see Table I) as reference targets.

Statistical analysis

The data were analyzed using SigmaStat 3.5 (Systat Software Inc.). Sample proportions were compared by 2-sample *z*-test; a nonparametric Mann–Whitney test was performed for Adhesion Score (0–3 point scale); relative gene expression values were compared by the Mann-Whitney *U* test; more-than-two-groups comparisons were done using ANOVA on ranks; $p < 0.05$ for the differences were considered statistically significant.

RESULTS
Mesh properties
Differences in structural and mechanical properties between PDO and PGA meshes are shown in Figure 1(a) and summarized in Table II.

In vitro cytotoxicity assay
The MTT-test results correspond to zero cytotoxicity of the materials [Figure 1(b)].

In vivo biocompatibility assay
All animals satisfactorily tolerated surgical intervention, and none of them died spontaneously. Moreover, none of the animals showed any signs of large hematoma, seroma, or abscess.

In the PDO and PGA groups, the meshes were rapidly pervaded by connective tissue of the host, becoming virtually inseparable from surrounding tissues as early as on day 10 after surgery. A comparable level of tissue integration for Permacol was shifted to later stages, at about 30 days after surgery; at earlier stages, the integration was limited and mostly confined to the perimeter of implant.

Adhesions of various degrees were observed in all groups at all time-points. In some of the animals, adhesion

TABLE I. PCR Primer Structures and Targets Definition

Target Symbol	Direction	Sequence (5′ to 3′)	NCBI Ref Seq	Target Definition
fgf2	Forw	CCAAGCGGCTCTACTGCAA	NM_019305.2	*Rattus norvegicus* fibroblast growth
	Rev	AGCCGTCCATCTTCCTTCATAG		factor 2 (Fgf2), mRNA
col1a1	Forw	CTGGCGCTTCAGGTCCAATG	NM_053304.1	*R. norvegicus* collagen, type I, alpha 1
	Rev	AGACCTCGGGGACCCATCT		(Col1a1), mRNA
mmp9	Forw	ATGGTTTCTGCCCCAGTGAG	NM_031055.1	*R. norvegicus* matrix metallopeptidase
	Rev	CACCAGCGATAACCATCCGA		9 (Mmp9), mRNA
timp1	Forw	CAGACAGCTTTCTGCAACTC	NM_053819.1	*R. norvegicus* TIMP metallopeptidase
	Rev	CACAGCGTCGAATCCTTTGA		inhibitor 1 (Timp1), mRNA
tnfa	Forw	CCACCACGCTCTTCTGTCTA	NM_012675.3	*R. norvegicus* tumor necrosis factor
	Rev	GCTACGGGCTTGTCACTCG		(Tnf), mRNA
tgfb	Forw	CCGCAACAACGCAATCTATG	NM_021578.2	*R. norvegicus* transforming growth
	Rev	AGCCCTGTATTCCGTCTCCTT		factor, beta 1 (Tgfb1), mRNA
il1b	Forw	CTGTCTGACCCATGTGAGCT	NM_031512.2	*R. norvegicus* interleukin 1 beta (Il1b),
	Rev	ACTCCACTTTGGTCTTGACTT		mRNA
il4	Forw	ATGTAACGACAGCCCTCTGA	NM_201270.1	*R. norvegicus* interleukin 4 (Il4), mRNA
	Rev	AGCACGGAGGTACATCACG		
il6	Forw	TACATATGTTCTCAGGGAGAT	NM_012589.2	*R. norvegicus* interleukin 6 (Il6), mRNA
	Rev	GGTAGAAACGGAACTCCAG		
il10	Forw	GCCCAGAAATCAAGGAGCAT	NM_012854.2	*R. norvegicus* interleukin 10 (Il10), mRNA
	Rev	TGAGTGTCACGTAGGCTTCTA		
actb	Forw	GAGATTACTGCCCTGGCTCC	NM_031144.3	*R. norvegicus* actin, beta (Actb), mRNA
	Rev	GCTCAGTAACAGTCCGCCTA		
b2m	Forw	CTCGCTCGGTGACCGTGAT	NM_012512.2	*R. norvegicus* beta-2 microglobulin (B2m),
	Rev	GGACAGATCTGACATCTCGA		mRNA
gapdh	Forw	GCGAGATCCCGCTAACATCA	NM_017008.4	*R. norvegicus* glyceraldehyde-3-phosphate
	Rev	CCCTTCCACGATGCCAAAGT		dehydrogenase (Gapdh), mRNA

formation affected not only the greater omentum, but also the loops of small and large intestine. The degree of adhesions was significantly higher in the Permacol group for all time-points except day 10 after surgery [Figure 2(a)].

Resorption rate evaluation and mechanical strength
All tested prostheses underwent resorption *in vivo*: the PGA filament size decreased by $41.5 \pm 2.1\%$, the Permacol thickness decreased by $32.0 \pm 2.9\%$ ($p < 0.05$), and the PDO

filament size decreased by $20.8 \pm 1.7\%$ ($p < 0.05$) as measured on histological sections of transplantation area on day 60 after surgery [Figure 2(b)].

Ultimate tensile strength (UTS) constituted 1.24 ± 0.26 MPa for freshly dissected full-thickness anterior abdominal wall fragments, 14.51 ± 2.10 MPa for the Permacol group on day 3 after surgery, and 1.25 ± 0.15 MPa for the Permacol group on day 10 after surgery, which is very similar to UTS of the freshly dissected fragments. UTS values for the
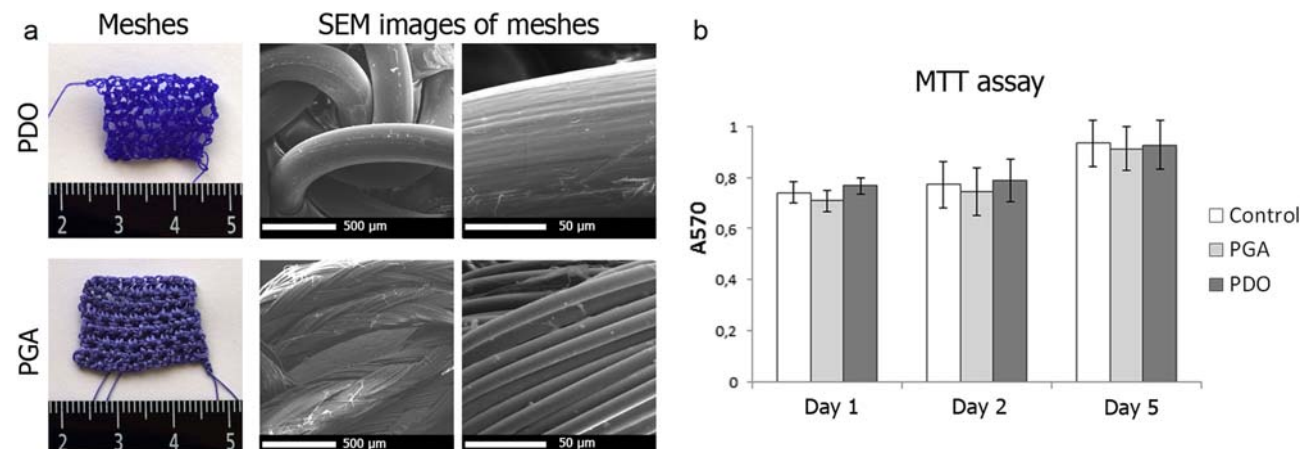
FIGURE 1. Mesh implants. Macroscopic optical images (left) and top-view SEM micrographs (right) (a) showing the architecture of PDO monofilament and PGA polyfilament meshes. Scale bars are 500 and 50 μm. The *in vitro* cytotoxicity MTT assay (b) showing the optical density at $\lambda = 570$ nm in wells containing human MSCs incubated for 1, 2, or 5 days in the presence of the PDO or PGA yarns. Wells with the cells only (no yarns) were used as a control. The data are presented as average $\pm$ SD. The MTT assay was repeated three times; the experimental results correspond to zero cytotoxicity of the materials.

TABLE II. Characteristics of the Meshes

Characteristics	PDO Mesh	PGA Mesh
Material	PDO	polyglycolic acid
Type of thread	Monofilament	Multifilament
Thread thickness, USP	3-0	3-0
Type of mesh	Woven	Woven
Shape of elements	Rectangular	Rectangular
Size of elements, mm	2.0–2.5	2.0–2.5
Tensile strength, MPa	5.01 ± 0.72	8.76 ± 0.97
Porosity, %	85.8	82.8
Microhardness, kgf/mm^2	35.2	52.0
Microhardness after hydrolytic degradation, kgf/mm^2	28.2	17.8
Size of mesh, mm	15×20	15×20
Expected resorption time, days	170–250	60–90

PDO and PGA groups also decreased gradually; characteristic mechanical indices for the three groups ultimately converged by day 30 after surgery [Figure 2(c)].

Histological examination

In the Permacol group, the boundary line between the transplant and the host tissues was clearly observed in histological sections of the Permacol group on day 10 after surgery, whereas in the PDO group at the same time-point individual monofilaments of the implant became overgrown by loose connective tissue, and in the PGA group elements of the tissue were observed within the multifilament, separating its units from one another (Figure 3).

The newly formed loose connective tissue was gradually replaced by dense irregular connective tissue. By day 60, in PDO and PGA groups all tissues contacting and penetrating the prosthesis were abundantly vascularized, whereas in the
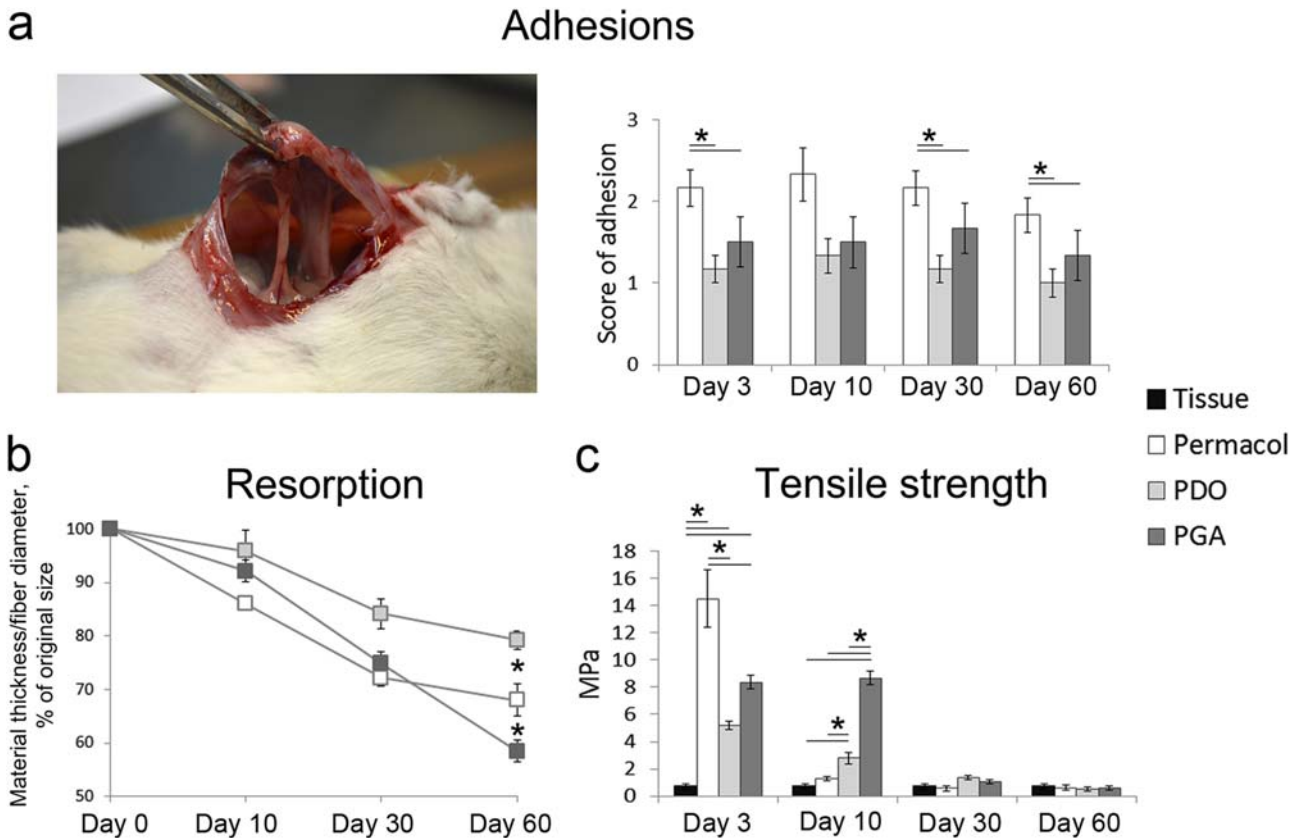
FIGURE 2. Biomechanical properties of the implants. Formation of abdominal adhesions (left) after mesh transplantation and quantification (right) of score of adhesion for PDO, PGA and Permacol groups (a). The degree of adhesions was significantly higher in the Permacol group than in the synthetic mesh groups. Quantification of implant material resorption (b) and tensile strength (c). The overall tensile strength of tissues at the surgical site decreased in all groups as long as the material was gradually resorbed, but the decrease was slower for the synthetic meshes than for Permacol. $n = 6$ per group at each time point. Values are expressed as average $\pm$ SD. * denotes significant difference ($p < 0.05$) between linked groups.
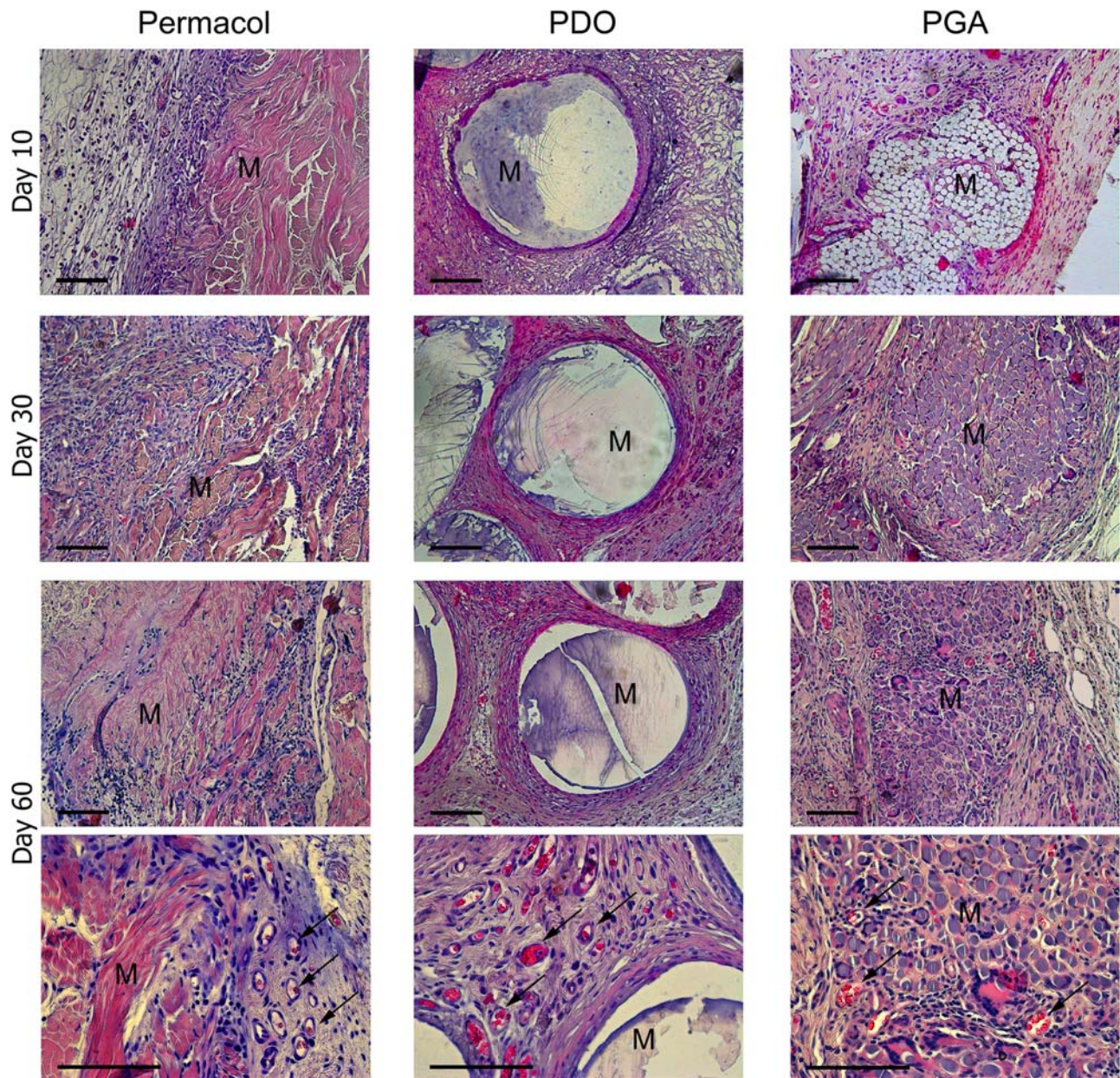
FIGURE 3. Representative images of H&E staining on day 10, 30, and 60 after the transplantation showing the integration between tissue and different mesh material. Histological examination confirmed the better integration of synthetic mesh prostheses into host environments as compared to Permacol. Arrows indicate blood vessels. By day 60, in PDO and PGA groups all tissues contacting and penetrating the prosthesis were abundantly vascularized, whereas in the Permacol group blood vessels were found only at peripheral sites with the highest degree of resorption. "M" denotes "Mesh material". Scale bars are 100 μm.

Permacol group blood vessels were found only at peripheral sites with the highest degree of resorption (Figure 3).

Also, on day 60, troponin I+ cells located diffusely and αSMA+ cells predominantly confined to blood vessel walls were observed in all groups [Figure 4(a)].

Collagen type I fibers associated with elements of the prosthesis were revealed as early as on day 3 after surgery; more of its fibers integrated into loose connective tissue surrounding the prosthesis were observed on day 10. Thickness of the collagen fibers and their bundles increased with maturation of the connective tissue. The fibers were oriented along the Permacol layer in the corresponding group, whereas in the PDO and PGA groups they tended to surround each individual filament of the prosthesis [Figure 4(a)].

Of genes involved in collagen synthesis or its regulation, *fgf2* and *col1a1* expression levels were high at the earlier time-points and gradually decreased until day 60 similarly in all groups. However, in the PDO group expression of *mmp9* gene was higher, and expression of its inhibitor-encoding gene *timp1* was lower, than in the other groups [Figure 4(b)].
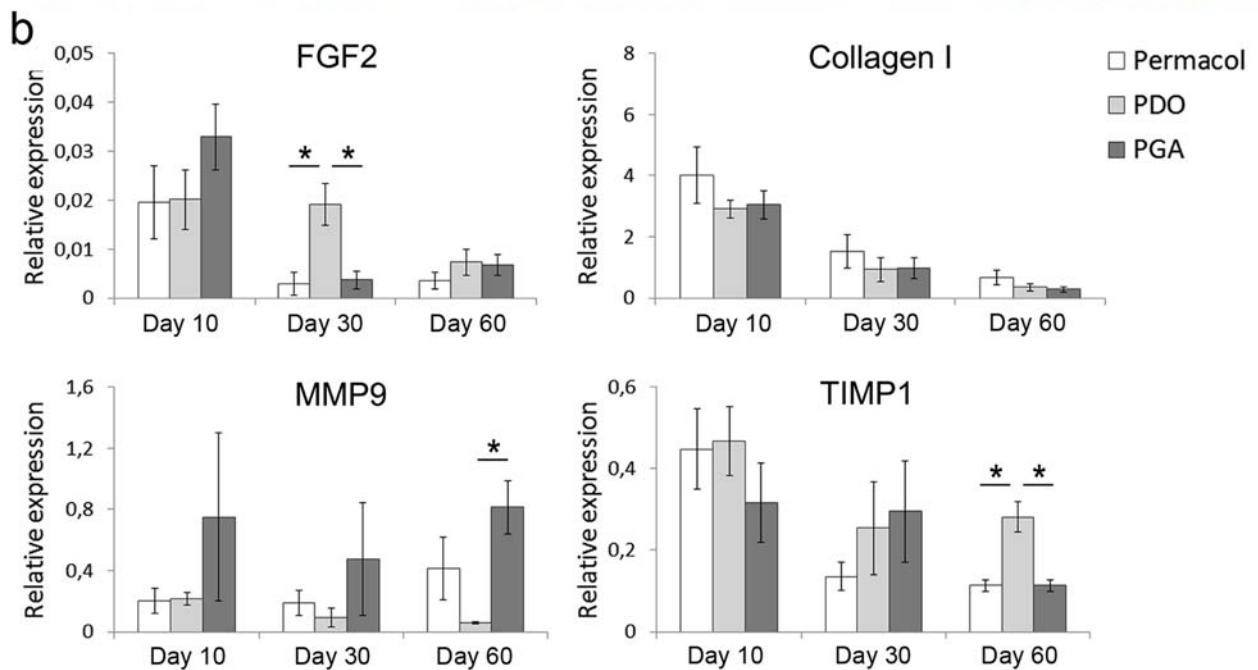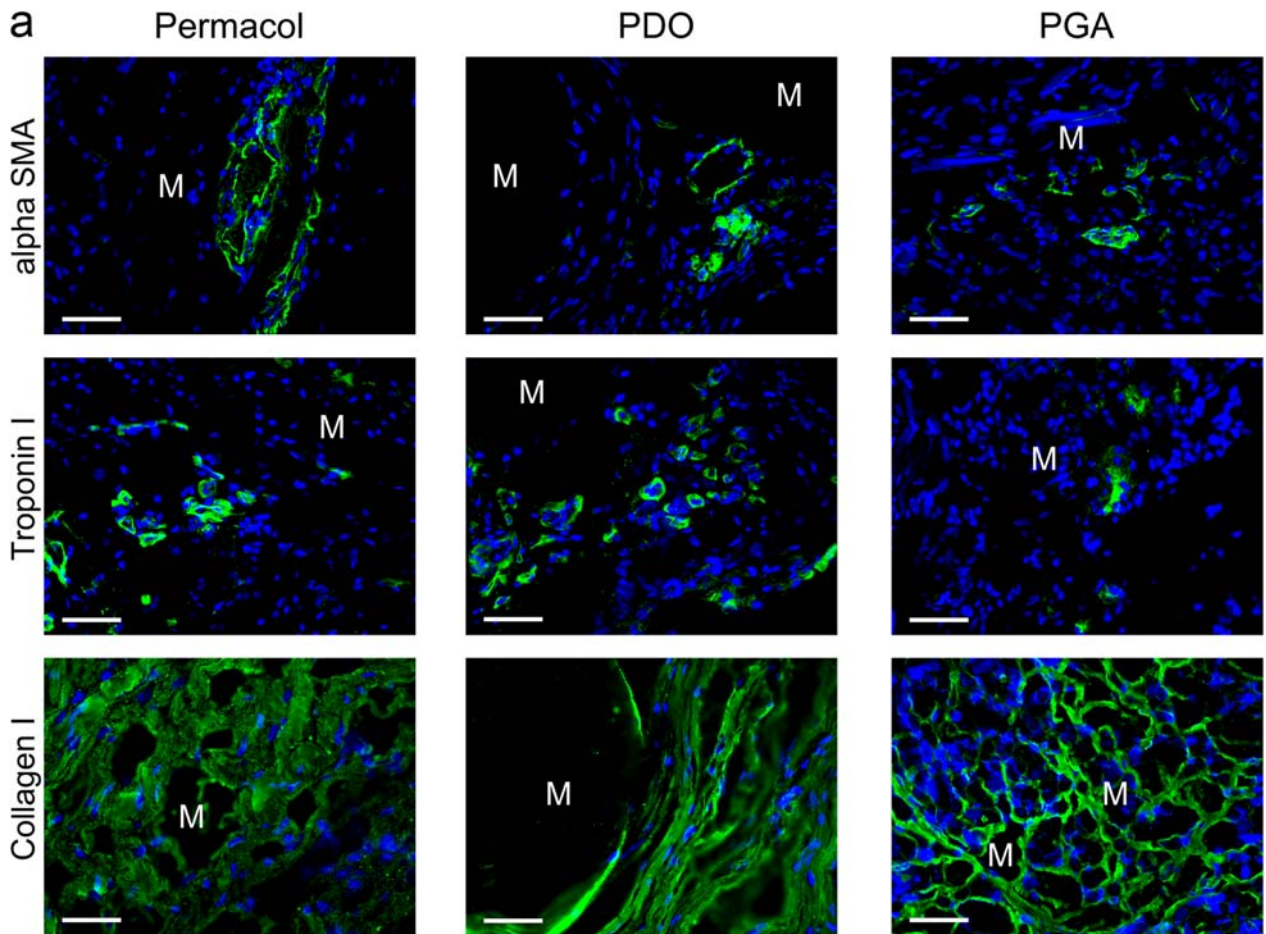
FIGURE 4. Peri-implant tissue remodeling. Representative images of IHC staining on day 60 after transplantation showing the localization of smooth muscle actin (green), troponin I (green) and type I collagen (green) (a). Cell nuclei were stained with DAPI (blue). "M" denotes "Mesh material." Scale bars are 50 μm. Relative expression levels of FGF2 and genes involved in extracellular matrix remodeling (b). Gene expression dynamics show that maximal rates of both production and remodeling of the matrix correspond to day 10, regardless of the type of prosthesis, but the PDO mesh transplantation is associated with accelerated maturation of the newly formed connective tissue. $n = 6$ per group at each time point. Values are expressed as average $\pm$ SD. * denotes significant difference ($p < 0.05$) between linked groups.
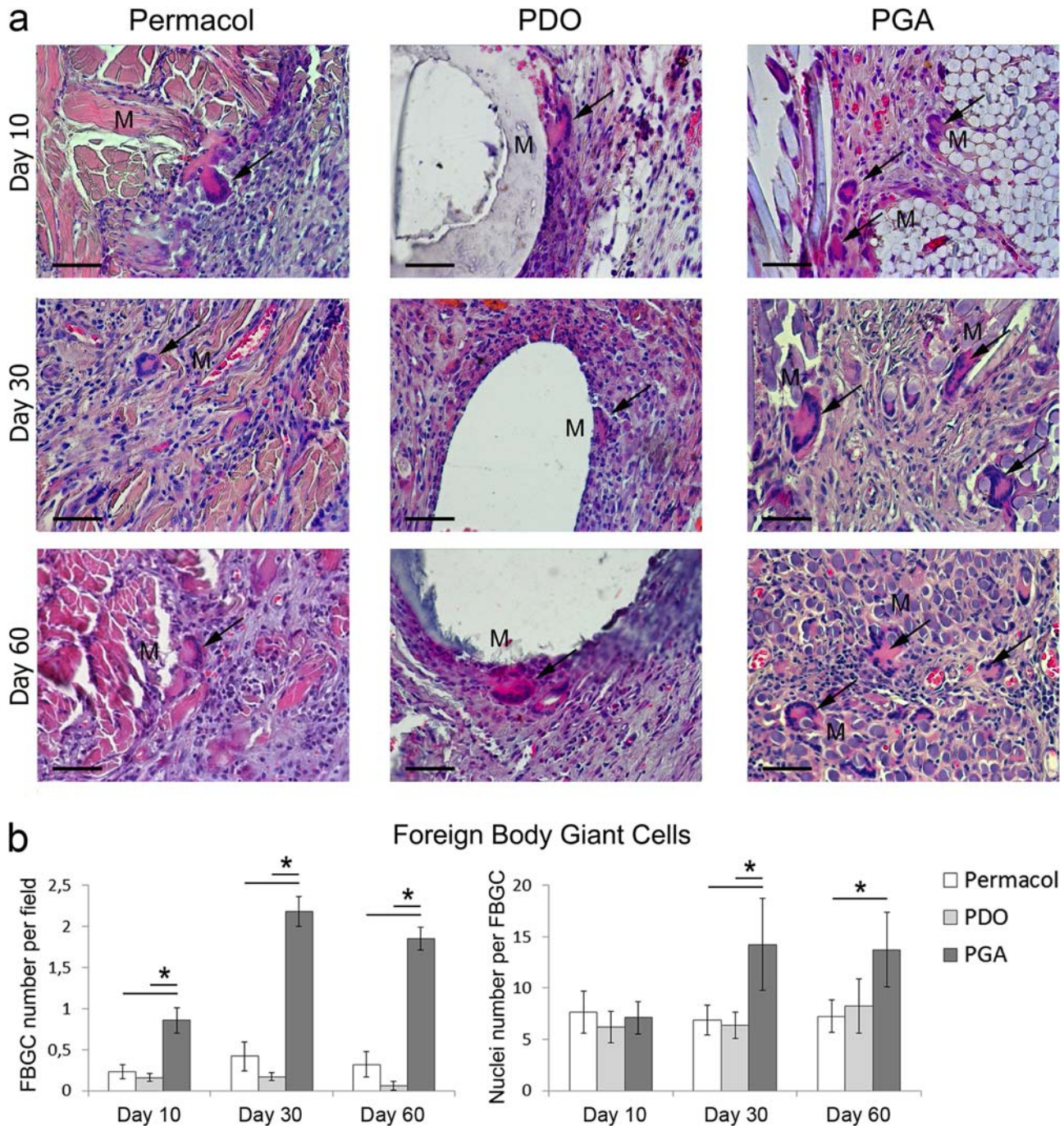
FIGURE 5. Foreign-body giant cell formation. Representative images of H&E staining on day 10, 30, and 60 after the transplantation showing the localization of foreign-body giant cells next to implant material (a). Arrows indicate foreign-body giant cells. "M" denotes "Mesh material". Scale bars are 50 μm. Quantitative assessment of FBGCs and the FGBC nuclei numbers (b). FBGCs were significantly more abundant and multi-nucleated in the PGA group. FBGCs were counted in 20 fields of view at 400× magnification for each animal individually. Values are expressed as average ± SD. * denotes significant difference ($p < 0.05$) between linked groups.

Evaluation of the foreign body inflammatory reaction

Diffusely distributed foreign body giant cells (FBGCs) were observed in all groups at all time-points [Figure 5(a)], but they never formed clusters (granulomas). In the PDO and Permacol groups FBGC numbers were low and did not change in the course of observation, while in the PGA group both the FBGC and the average FGBC nuclei numbers increased significantly by day 30 and remained high until day 60 [Figure 5(b)].

Macrophage infiltration of the site by CD68+ cells was prominent in all groups, with the macrophages found predominantly in close vicinity of the prostheses [Figure 6(a)]. On day 10, the macrophage presence was significantly higher in the Permacol group, and on day 60—in the PGA
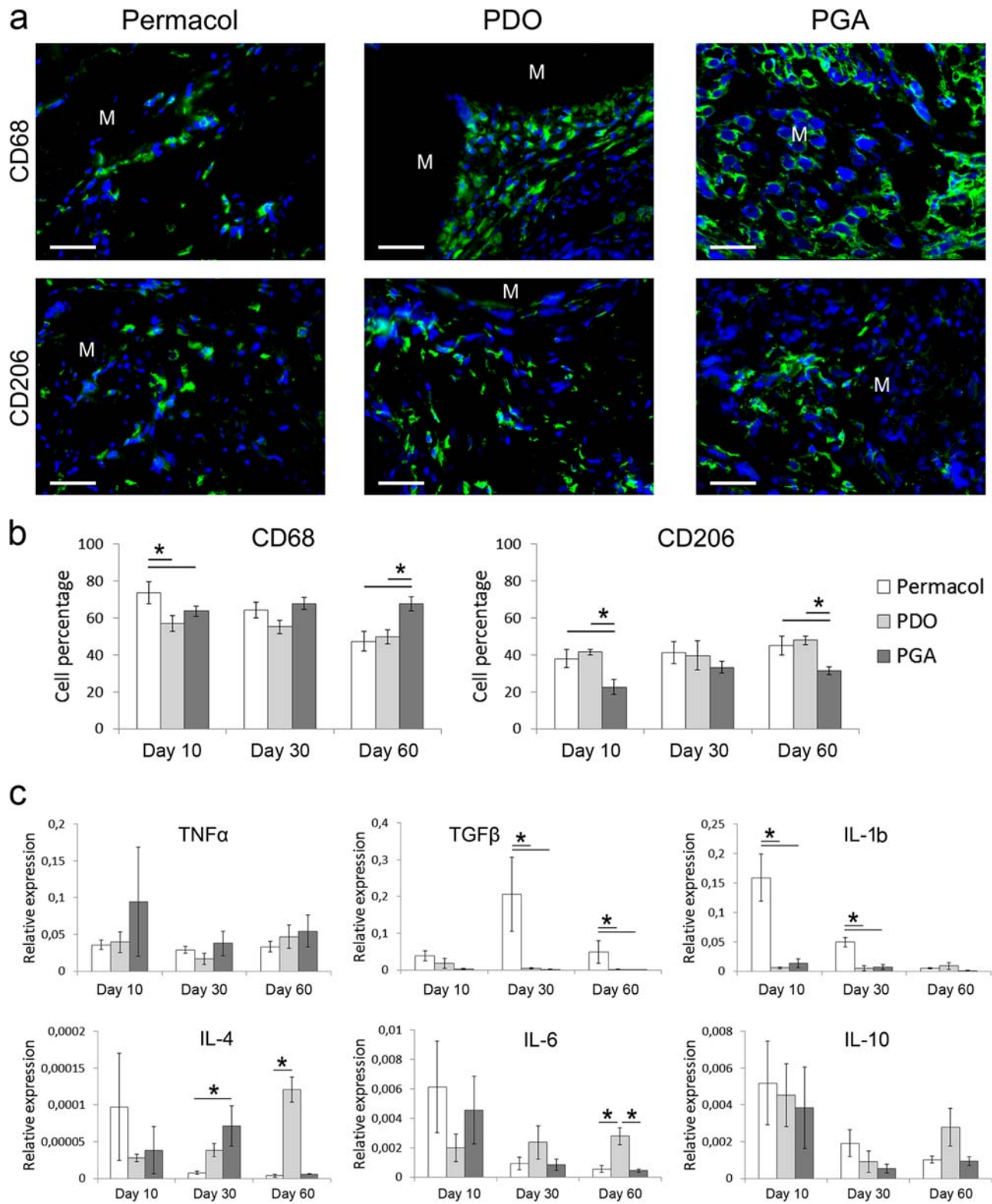
FIGURE 6. Inflammatory response of host tissues to the mesh implantation. Representative images of IHC staining on day 60 after surgery showing the localization of CD68+ cells CD206+ cells (green) (a). Macrophages are predominantly observed in the close vicinity of the prostheses. CD68 is a marker of total macrophage population and CD206 is a marker of alternatively activated macrophages exhibiting anti-inflammatory functions. Cell nuclei were stained with DAPI (blue). "M" denotes "Mesh material". Scale bars are 50 μm. Quantitative assessment of macrophage infiltration (b). The proportion of CD68+ or CD206+ cells among total cells were counted in 20 fields of view at 400× magnification for each animal individually. Values are expressed as average ± SD. * denotes significant difference ($p < 0.05$) between linked groups. M2-polarized macrophages were underrepresented in the PGA group, which can be regarded as a drawback of this type of prosthesis. Relative Expression levels of pro-inflammatory and anti-inflammatory cytokines (c). Gene expression dynamics indicates more profound and prolonged inflammatory reaction in response to Permacol than to synthetic mesh implants. $n = 6$ per group at each time point. Values are expressed as average ± SD. * denotes significant difference ($p < 0.05$) between linked groups.

group, with almost all filaments of the prosthesis densely encompassed by macrophages [Figure 6(b)].

M2-macrophages, defined as CD206+ cells, were also located predominantly in the connective tissue capsule around the prosthesis [Figure 6(a)]. Their abundance was significantly lower in the PGA group on days 10 and 60 after surgery, as compared with the other two groups at the same time-points [Figure 6(b)].

Local expression dynamics of genes encoding principal signal molecules that regulate alterative and productive phases of inflammation (exemplified by TNFα and TGFβ, respectively) was analyzed by PCR. The *tnfα* mRNA expression was found to be constant, that is, its levels were similar in all groups and between the time-points. The *tgfβ* expression significantly increased in the Permacol group by day 30 and decreased later on, still remaining significantly higher than in the other two groups by day 60. The pro-inflammatory cytokine *il1b* gene expression also increased in the Permacol group on days 10 and 30, as compared with PDO and PGA groups at these time-points [Figure 6(c)].

The anti-inflammatory cytokine *il4* and *il6* gene expression levels were significantly higher in the PDO group than in the Permacol and PGA groups on day 60 after surgery [Figure 6(c)].

DISCUSSION

For more than half a century, researchers have been looking for the ideal material for hernioplasty: many studies have been published that analyze effectiveness and safety of prosthetics in connection with the origin of the material (biological vs. synthetic), rate of resorption, structure (mono- vs. multi-filament), and so forth.[1,2,9–11]

The advantages of using resorbable/biodegradable prostheses instead of non-resorbable prostheses are questionable.[9,10] On one hand, the prosthesis represents a physical cause of various postoperative complications such as fibrosis, chronic pains, and fistula formation; therefore, its complete dissolution is favorable. On the other hand, mechanical inconsistency of the replacing tissues may increase the risks of recurrence. Resorbable prostheses are contraindicated in patients with compromised collagen synthesis; their use in the inguinal hernia treatment is generally unadvisable. Hernias of other location, however, can be effectively treated with resorbable prostheses, which ensure only temporal (1 to 3 months) reinforcement of the affected area, while promoting its pervasion with the patient's own tissues. The resorbable prostheses proved to be a particularly good choice in the incisional hernia prevention.

The main advantage of the resorbable/biodegradable synthetic meshes over the decellularized tissue-based matrices is their high porosity, which promotes the tissue ingrowth and ultimately reduces the risks of recurrence. An additional advantage is conferred by rapidly developing techniques of loading the material with growth factors or living cells. Such modifications can substantially elevate the rates of replacement.

The trend of using resorbable prostheses in hernioplasty is still weak and underdeveloped. Recent achievements in materials science, especially in obtaining polymers and designs with tunable physico-chemical properties and variable rates of resorption, will help to optimize choices of treatment specifically for any given case. However, the truly personalized approach will only result from extensive clinical studies. The limited usefulness of animal models in this particular case is exacerbated by the unavailability of spontaneous hernia formation in rodents.

With all the variety of prostheses currently in use, the high frequency of mesh-associated complications, which are specifically determined by intrinsic properties of the implant, still represents a major problem. For example, it is believed that the risk of infection is mainly determined by the type of filament used and the pore size: the meshes at lowest risk of infection are those made with monofilament and containing pores >75 μm.[19] Given this, the lower risks of infection for the monofilament PDO prosthesis could be predicted.

It is known that all meshes produce adhesions when placed adjacent to bowel,[19] but the degree of adhesion formation appears to be largely determined by intrinsic properties of the prosthesis. In this study, the biological prosthesis Permacol induced intense fibrotic reaction ensured strong adherence of the bowel to the abdominal wall and to the newly formed connective tissue [Figure 2(a)], whereas the synthetic meshes proved to be better in this respect.

On the other hand, Permacol had significantly higher initial strength characteristics [Figure 2(c)], which is consistent with the previously published data on the supreme mechanical strength of natural biological matrices: 15.7 MPa for dermal allograft[20] and 22.4 MPa for intestinal submucosa.[21] However, when using completely resorbable prostheses, it is not the physical or mechanical properties themselves that are important, but their dynamics as the prosthesis is resorbed and replaced by the host tissues. The strength of biological prostheses significantly decreases even when the material is moistened (e.g., for the single-layered small intestine submucosa this index decreases from 20.6 to 7.2 MPa[21]) and even more so in the course of *in vivo* remodeling.[20] In our experiments, the overall tensile strength of tissues at the surgical site decreased in all groups as long as the material was gradually resorbed, but the decrease was slower for the synthetic meshes than for Permacol [Figure 2(b)]. The lower rates of resorption in the PDO group correlated with the differential decrease in filament microhardness following hydrolytic destruction (Table II). The difference in rates of resorption could be explained not only by the difference in chemical composition of the prostheses, but also by the difference in the area of their contact with host tissues, which was much greater for the PGA multifilaments than for the PDO monofilaments.

Histological examination confirmed the better integration of synthetic mesh prostheses into host environments as compared to Permacol (Figure 3). The low efficacy of blood

vessel ingrowth into Permacol *in vivo* has already been noted by other authors.[22]

The data on expression of genes, which participate in the extracellular matrix production or digestion, show that maximal rates of both production and remodeling of the matrix correspond to day 10, regardless of the type of prosthesis. However, the PDO group differed from the other two groups by prolonged *fgf2* expression (until day 30), as well as a significant decrease in *mmp9* expression and simultaneous increase in *timp1* expression by day 60. It is plausible that the PDO mesh transplantation was associated with accelerated maturation of the newly formed connective tissue (Figure 4), whereas in the other groups it remained susceptible to remodeling for a longer period.

Another important characteristics of prostheses, related to both spatial organization and chemical composition of the material, is the severity of the foreign body-induced inflammatory reaction. It is known that larger transplants (in respect to cell size) behave as foreign bodies by causing activation of innate immunity, primarily the macrophages, which actively migrate toward the implanted prosthesis, subsequently proliferate, and differentiate into FBGCs. These cells, together with mononuclear leukocytes, accumulate around the foreign body where they may produce clusters called non-immune (non-specific) granulomas. These clusters are exterminated later on by encapsulation, to be replaced by fibrous tissue; however, in case of the foreign body persistence (e.g., for non-resorbable prostheses) they may be preserved for a lifetime.[7,23]

Although in our setting FBGCs were observed for all types of the prosthesis [Figure 5(a)], in the PGA group they were significantly more abundant and multinucleated [Figure 5(b)]. The rates of macrophage fusion (which is the way the FBGCs are formed) may depend on size of particles released during resorption of the prosthesis: if the particle size is larger than 10 μm and smaller than 100 μm, the macrophages fuse together, forming giant cells which in turn engulf the particles and digest them.[24] In the PDO group the filament diameter was rather large (about 330 μm), while in the PGA group it was only about 11 μm, which provided the optimal conditions for the fusion.

To characterize the inflammatory reaction, we evaluated relative counts of total macrophages (CD68+ cells) and M2-polarized macrophages (CD206+ cells) [Figure 6(a)]. By producing large quantities of growth factors and anti-inflammatory cytokines, the M2-polarized macrophages actively stimulate repair processes, extracellular matrix remodeling, and angiogenesis.[25] It is generally accepted that the presence of M2-polarized macrophages in the implant environment correlates with positive healing outcomes.[26] In particular, the M2-polarized macrophages were underrepresented in the PGA group, which can be regarded as a drawback of this type of prosthesis [Figure 6(b)].

In the Permacol group, macrophage infiltration at early time-points was more pronounced and *il1b* expression level was higher than in other groups, and increased expression of *tgfb* on later stages was typical [Figure 6(c)]. Such a character of gene expression dynamics indicates more profound and prolonged inflammatory reaction in response to Permacol, which is basically decellularized porcine dermis, than to synthetic mesh implants.

Thus, we invariably observed the transplant rejection, which developed gradually by means of innate immunity with subsequent full-scale foreign body inflammatory reaction and resulted in formation of fibrous capsule around residual elements of the resorbing prosthesis. These stages of the foreign body reaction are interconnected, and specific details of each stage depend on the history of preceding stages[27] and, ultimately, on the properties of the implanted material, which makes the reasonable choice of prosthetic material extremely important.

CONCLUSION

Biocompatibility and efficacy of experimental samples of mesh implants based on PGA or PDO were tested *in vitro* and *in vivo* against the commercial Permacol prosthetic material widely used in surgery and obtained from the decellularized dermis of pigs. In rat model of abdominal wall excisional defect repair, all tested types of the prostheses were gradually resorbed and replaced with host connective tissue containing elements of skeletal muscle histogenesis. As the mechanical strength of the prosthesis decreased due to its resorption, overall mechanical strength of the abdominal wall at the site of intervention was maintained comparable to the intact abdominal wall strength values in all groups.

By a number of indicators of biocompatibility and efficacy (adhesion formation severity, inflammatory reaction, activation of the anti-inflammatory and regeneration-supporting M2 macrophages), the PDO prosthesis turned out to be significantly better than the PGA prosthesis or Permacol.

The developed resorbable mesh prosthesis composed of PDO monofilaments can be further considered for the abdominal wall volume defect filling and the pelvic floor reinforcement.

CONFLICT OF INTEREST

The authors declare that they have no conflict of interest.

ETHICAL APPROVAL

All applicable international, national, and/or institutional guidelines for animal care were followed. All procedures performed in the studies involving animals were in accordance with the ethical standards of the institution or practice at which the studies were conducted.

HUMAN AND ANIMAL RIGHTS

All animals were treated in accordance with the Guide for the Care and Use of Laboratory Animals. This article does not contain any studies with human participants performed by any of the authors.

INFORMED CONSENT

For this type of study informed consent was not required.

REFERENCES

1. Bilsel Y, Abci I. The search for ideal hernia repair; mesh materials and types. Int J Surg 2012;10(6):317–321.
2. Baylón K, Rodríguez-Camarillo P, Elías-Zúñiga A, Díaz-Elizondo JA, Gilkerson R, Lozano K. Past, present and future of surgical meshes: A review. Membranes 2017;7(3): E47.
3. Maher C, Feiner B, Baessler K, Schmid C. Surgical management of pelvic organ prolapse in women. Cochrane Database Syst Rev 2013;4:CD004014.
4. den Hartog D, Dur AH, Tuinebreijer WE, Kreis RW. Open surgical procedures for incisional hernias. Cochrane Database Syst Rev 2008;3:CD006438.
5. Eriksen JR, Gögenur I, Rosenberg J. Choice of mesh for laparoscopic ventral hernia repair. Hernia 2007;11(6):481–492.
6. Sadava EE, Krpata DM, Gao Y, Rosen MJ, Novitsky YW. Wound healing process and mediators: Implications for modulations for hernia repair and mesh integration. J Biomed Mater Res A 2014; 102(1):295–302.
7. Lacour M, Ridereau Zins C, Casa C, Venara A, Cartier V, Yahya S, Barbieux J, Aubé C. CT findings of complications after abdominal wall repair with prosthetic mesh. Diagn Interv Imaging 2017;98(7–8):517–528.
8. Salamone G, Licari L, Agrusa A, Romano G, Cocorullo G, Gulotta G. Deep seroma after incisional hernia repair. Case reports and review of the literature. Ann Ital Chir 2015;86(ePub). pii: S2239253X15022938.
9. Darehzereshki A, Goldfarb M, Zehetner J, Moazzez A, Lipham JC, Mason RJ, Katkhouda N. Biologic versus nonbiologic mesh in ventral hernia repair: A systematic review and meta-analysis. World J Surg 2014;38(1):40–50.
10. Majumder A, Winder JS, Wen Y, Pauli EM, Belyansky I, Novitsky YW. Comparative analysis of biologic versus synthetic mesh outcomes in contaminated hernia repairs. Surgery 2016;160(4):828–838.
11. Fang Z, Ren F, Zhou J, Tian J. Biologic mesh versus synthetic mesh in open inguinal hernia repair: System review and meta-analysis. ANZ J Surg 2015;85(12):910–916.
12. Lucke S, Hoene A, Walschus U, Kob A, Pissarek J-W, Schlosser M. Acute and chronic local inflammatory reaction after implantation of different extracellular porcine dermis collagen matrices in rats. Biomed Res Int 2015;2015:938059.
13. Koontz AR, Kimberly RC. Further experimental work on prostheses for hernia repair. Surg Gynecol Obstet 1959;109:321.
14. Ruiz-Jasbon F, Norrby J, Ivarsson ML, Björck S. Inguinal hernia repair using a synthetic long-term resorbable mesh: Results from a 3-year prospective safety and performance study. Hernia 2014; 18(5):723–730.
15. Herold A, Ommer A, Fürst A, Pakravan F, Hahnloser D, Strittmatter B, Schiedeck T, Hetzer F, Aigner F, Berg E, Roblick M, Bussen D, Joos A, Vershenya S. Results of the Gore Bio-A fistula plug implantation in the treatment of anal fistula: A multicentre study. Tech Coloproctol 2016;20(8):585–590.
16. Scott JR, Deeken CR, Martindale RG, Rosen MJ. Evaluation of a fully absorbable poly-4-hydroxybutyrate/absorbable barrier composite mesh in a porcine model of ventral hernia repair. Surg Endosc 2016;30(9):3691–3701.
17. Scott G. Degradable Polymers, Second Edition: Principles and Applications. Amsterdam: Kluwer Academic Publishers; 2003.
18. Costa RG, Lontra MB, Scalco P, Cavazzola LT, Gurski RR. Polylactic acid film versus acellular porcine small intestinal submucosa mesh in peritoneal adhesion formation in rats. Acta Cir Bras 2009; 24(2):128–135.
19. Brown CN, Finch JG. Which mesh for hernia repair? Ann R Coll Surg Engl 2010;92(4):272–278.
20. Ngo MD, Aberman HM, Hawes ML, Choi B, Gertzman AA. Evaluation of human acellular dermis versus porcine acellular dermis in an in vivo model for incisional hernia repair. Cell Tissue Bank 2011;12(2):135–145.
21. Shi L, Ronfard V. Biochemical and biomechanical characterization of porcine small intestinal submucosa (SIS): A mini review. Int J Burns Trauma 2013;3(4):173–179.
22. Mimura KK, Moraes AR, Miranda AC, Greco R, Ansari T, Sibbons P, Greco KV, Oliani SM. Mechanisms underlying heterologous skin scaffold-mediated tissue remodeling. Sci Rep 2016;6:35074.
23. Junge K, Binnebösel M, von Trotha KT, Rosch R, Klinge U, Neumann UP, Lynen Jansen P. Mesh biocompatibility: Effects of cellular inflammation and tissue remodelling. Langenbecks Arch Surg 2012;397(2):255–270.
24. Sheikh Z, Brooks PJ, Barzilay O, Fine N, Glogauer M. Macrophages, foreign body giant cells and their response to implantable biomaterials. Materials (Basel) 2015;8(9):5671–5701.
25. Mills CD. M1 and M2 macrophages: Oracles of health and disease. Crit Rev Immunol 2012;32(6):463–488.
26. Sridharan R, Cameron AR, Kelly DJ, Kearney CJ, O'Brien FJ. Biomaterial based modulation of macrophage polarization: A review and suggested design principles. Mater Today 2015;18(6):313–325.
27. Wong ML, Wong JL, Vapniarsky N, Griffiths LG. In vivo xenogeneic scaffold fate is determined by residual antigenicity and extracellular matrix preservation. Biomaterials 2016;92:1–12.